arXiv:hep-ph/0312359v2 9 Jan 2004

LAPTH 1020/03
IMSc-2003/11/35
LPT-Orsay 03-97
IISc-CTS/18/03
December 2003

An NLO calculation of the electroproduction of large-$E_\perp$ hadrons

P. Aurenche[a], Rahul Basu[b], M. Fontannaz[c], R.M. Godbole[d]

[a] *LAPTH, UMR 5108 du CNRS associée à l'Université de Savoie, BP 110, Chemin de Bellevue, 74941 Annecy-le-Vieux Cedex, France*

[b] *The Institute of Mathematical Sciences, Chennai 600 113, India*

[c] *Laboratoire de Physique Théorique, UMR 8627 CNRS, Université Paris XI, Bâtiment 210, 91405 Orsay Cedex, France*

[d] *Centre for Theoretical Studies, Indian Institute of Science, Bangalore 560012, India*

Abstract

We present a Next-to-Leading Order calculation of the cross section for the leptoproduction of large-$E_\perp$ hadrons and we compare our predictions with H1 data on the forward production of π^0. We find large higher order corrections and an important sensitivity to the renormalization and factorization scales. These large corrections are shown to arise in part from BFKL-like diagrams at the lowest order.

1 Introduction

The electroproduction of large-$E_\perp$ hadrons which is observed by the HERA experiments H1 [1, 2, 3] and ZEUS [4] may provide important tests of QCD. In addition to the study of the partonic subprocesses, of the parton distributions in the proton and of the fragmentation functions, it also offers the possibility to observe the virtual photon structure function. A contribution of the latter is indeed expected when the hadron transverse energy squared $E_\perp^2$ is much larger than the photon virtuality $Q^2 = |q^2|$; in this case the virtual photon structure function contribution, proportional to $\log \frac{E_\perp^2}{Q^2}$, can be important.

Another interest of this reaction is the study of the production mechanisms of forward hadrons. Indeed, the forward region can be associated with BFKL dynamics and provide tests of the latter [5]. Several papers have studied the production of large-$E_\perp$ jets [6] and hadrons [7] in the forward direction, and have concluded that these reactions are relevant for the study of BFKL dynamics. However, results from H1 [2] show that theoretical predictions based on the DGLAP dynamics, implemented in RAPGAP [8] or based on BFKL dynamics [9] are both in agreement with data. These theoretical results do not necessarily contradict each other, since the same Feynman graphs may contribute to both of them. But it is clear that a deeper understanding of the underlying forward dynamics requires quantitative predictions, which are not fully realized in the existing literature above. Ref. [8] which implements the DGLAP dynamics rests on a Leading Order (LO) approximation and suffers from scale dependence which forbids an absolute normalization. Ref. [9] takes into account some Higher Order (HO) corrections to the LO BFKL equation, but does not include non-BFKL contributions.

In this paper we calculate the HO corrections to the Born subprocesses associated with the electroproduction of large-$E_\perp$ hadrons namely the QCD Compton process $\gamma^* + q \to g + q$ and the fusion process $\gamma^* + g \to q + \bar{q}$. The Born subprocess cross

sections, of order $\mathcal{O}(\alpha\alpha_s)$, and the HO subprocess cross sections, of order $\mathcal{O}(\alpha\alpha_s^2)$, are convoluted with parton distributions and fragmentation functions calculated at the NLO approximation. The total NLO cross-section (Born + HO contributions) is sensitive to the choice of the renormalization and factorization scales, but there is a compensation between the variations of the Born and HO contributions in such a way that the NLO cross section is more stable than the LO (containing only the Born terms) cross sections.

The work presented here is a fixed order (for the subprocess cross section), NLO calculation, the DGLAP dynamics being included by the scale dependent distributions and fragmentation functions. However, among the HO contributions, one of them corresponds to the lowest order BFKL cross section, namely, the reaction $\gamma^* + g \to g + q + \bar{q}$. As this contribution is part of an HO calculation, we have a way to establish a link between the normalization of our NLO cross section and that of the (lowest order) BFKL cross section.

As mentioned in the beginning of this section, the HO calculation generates a contribution proportional to the virtual photon structure function. At order $\mathcal{O}(\alpha\alpha_s^2)$ we obtain the Born expression of this structure function, proportional to $\log E_\perp^2/Q^2$ and we shall study how important this contribution to the large-$E_\perp$ forward hadron cross section is in the H1 kinematical configuration. All order contributions to the virtual photon structure function can be resummed using an inhomogeneous DGLAP evolution equation. Here we shall briefly discuss this possibility, leaving for another publication [10] a detailed analysis of the resummed virtual photon structure function.

As a final point concerning the nature of this calculation, let us emphasize the fact that it describes the production of large-$E_\perp$ hadrons in the virtual-photon proton centre-of-mass system (CMS) and that it is also valid in the limit $Q^2 = 0$, the large scale then being provided by $E_\perp^2$. It must be compared with experimental results which impose a lower bound on the final hadron $E_\perp$ in the $\gamma^* - P$ CMS, as is done

by the H1 and ZEUS collaboration [2, 3, 4]. Therefore the present work does not consider the target fragmentation mechanism, which requires the introduction of fracture functions [11, 12, 13, 14]. It is also different from the inclusive calculations of ref. [13, 14] in that it is an exclusive NLO partonic generator. This allows us to calculate various types of correlations (for example between large-$E_\perp$ hadron and jets) and facilitates the implementation of experimental cuts.

In the next section we shall present an overview of the relevant DIS kinematics and of the method used to calculate the HO corrections. Section 3 is devoted to a discussion of the virtual photon structure function and, in section 4, we compare our theoretical results with H1 data [2]. We shall discuss in detail the importance of the virtual photon contribution and of the BFKL-like contribution in the H1 kinematical region. Section 5 studies the production of large-$E_\perp$ hadrons in the central region in rapidity. Section 6 is the conclusion.

2 The NLO calculation

The kinematics of the reaction $e(\ell) + p(P) \to e(\ell') + h(P_4) + X$ is fixed by the observation, in the laboratory frame, of the outgoing lepton and hadron h momenta [2]. We define the photon variables (axis Oz along the initial proton momentum)

$$\begin{aligned} Q^2 &= -q^2 = -(\ell - \ell')^2 \\ y &\equiv \frac{q^{(-)}}{\ell^{(-)}} = \frac{q^0 - q^z}{\ell^0 - \ell^z} = \frac{P \cdot q}{P \cdot \ell} = \frac{Q^2}{S} \, \frac{1}{x_{Bj}}, \end{aligned} \tag{1}$$

where we have neglected the proton mass and used the notation $S = (\ell + P)^2$ and $x_{Bj} = \frac{Q^2}{2P \cdot q}$. The outgoing hadron is defined by its transverse energy $E_{\perp 4}^{Lab}$ and its pseudo rapidity η_4^{Lab}.

The inclusive cross section is written in terms of the leptonic tensor (summed and averaged over the spins of the leptons)

$$\ell^{\mu\nu} = 2\left(\ell^{\mu}\ell'^{\nu} + \ell'^{\mu}\ell^{\nu} - g^{\mu\nu}\left(\ell\cdot\ell' - m_e^2\right)\right), \tag{2}$$

and the hadronic tensor $T_{\mu\nu}$ which describes the photon-proton collision

$$\frac{d\sigma}{d\varphi dQ^2 dy} = \frac{\alpha}{2\pi}\,\frac{1}{2\pi}\,\frac{1}{2S}\int\frac{1}{2}\,\frac{\ell^{\mu\nu}T_{\mu\nu}}{q^4}dPS, \tag{3}$$

where

$$dPS = (2\pi)^4\delta^4\left(q + P - \sum_{i=1}^{n} p_i\right)\prod_{i=1}^{n}\frac{d^4p_i}{(2\pi)^3}\delta(p_i^2)\theta(p_i^0)$$

is the final state hadron phase space element and φ the photon azimuthal angle. (A sum over the number of final hadrons is understood in (3)).

The hadronic tensor can be calculated as a convolution between the partonic tensor $t_{\mu\nu}$ which describes the interaction between the virtual photon and the parton of the proton, and the parton distribution in the proton $G_a(x, M)$. The fragmentation of the final parton which produces a large-$E_\perp$ hadron is described by the fragmentation function $D_b^h(z, M_F)$. These distributions depend on the factorization scales M and M_F,

$$\int T_{\mu\nu}dPS = \sum_{a,b}\int\frac{dx}{x}G_a(x,M)\int dz\; D_b^h(z,M_F)t_{\mu\nu}^{ab}\cdot dps, \tag{4}$$

where dps is the phase space element of the partons produced in the hard photon-parton collision. From expressions (3) and (4), we obtain

$$\frac{d\sigma}{d\varphi dQ^2 dy dE_{\perp 4}^{Lab} d\eta_4^{Lab}} = \frac{E_{\perp 4}^{Lab}}{2\pi}\frac{\alpha}{2\pi}\sum_{a,b}\int dx G_a(x,M)\int\frac{dz}{z^2}D_b^h(z,M_F)$$
$$\int\frac{d\varphi_4^{Lab}}{2\pi}\frac{1}{(4\pi)^2}\frac{1}{2xS}\frac{\ell^{\mu\nu}t_{\mu\nu}^{ab}}{q^4}dps', \tag{5}$$

where the phase space dps' no longer contains parton 4 which fragments into $h(P_4)$. Up to this point we have been writing $E_{\perp 4}^{Lab}$ and η_4^{Lab} to emphasize the frame in

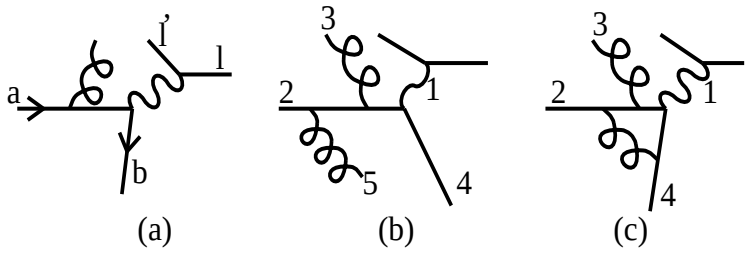

Figure 1: The QCD Compton subprocess (Fig. 1a) and real (virtual) HO corrections to it (Fig. 1b (Fig. 1c)).

which the reaction is observed. Of course (5) is valid in any frame and from now on we shall drop the index "Lab".

The tensor product is a series in α_s. Taking into account the first and second order contributions, we rewrite (5) as

$$\frac{d\sigma}{d\varphi dQ^2 dy dE_{\perp 4} d\eta_4} = \frac{\alpha}{2\pi} \sum_{a,b} \int dx G_a(x,M) \int \frac{dz}{z^2} D_b^h(z,M_F)$$
$$\left\{ \frac{\alpha_s(\mu)}{2\pi} \frac{d\widehat{\sigma}_{a,b}^{Born}(x,z)}{d\varphi dQ^2 dy dE_{\perp 4} d\eta_4} + \left(\frac{\alpha_s(\mu)}{2\pi}\right)^2 \frac{dK_{ab}^{HO}(x,z,\mu,M,M_F)}{d\varphi dQ^2 dy dE_{\perp 4} d\eta_4} \right\} . \qquad (6)$$

The cross sections $\widehat{\sigma}_{ab}^{Born}$ are the subprocess Born cross sections which describe the electroproduction of a large-$E_\perp$ parton b and K_{ab}^{HO} are the associated Higher Order corrections.

Figure 1a shows the Born term corresponding to the QCD Compton (QCDC) process (here partons a and b are quarks). When a is a gluon, we have the so called photon-gluon fusion Born term. Examples of a graph contributing to HO corrections to the QCDC term are shown in Fig. 1b, c. (The numbers 1 to 5 label the initial and final partons according to a convention used in the HO calculations described below).

In expression (6) we have explicitly written the dependence of the cross section

on the strong coupling constant $\alpha_s(\mu)$ which depends on the renormalization scale μ.

It is convenient to perform the calculation of $\widehat{\sigma}^{Born}$ and K^{HO} in the virtual photon-proton center of mass system, and from now on we shall work in this frame. In fact, the H1 collaboration explicitly uses this frame to place cuts on the outgoing hadron transverse momentum. We take the positive Oz axis along the proton momentum (as per the H1 convention) and the leptons are contained in the Oxz-plane.

It is instructive to give a more explicit form to the tensor product in the $\gamma^* - p$ frame using expression (2) and defining the transverse polarization vectors $\varepsilon_1^\mu = (0,1,0,0)$, $\varepsilon_2^\mu = (0,0,1,0)$ and the scalar polarization vector $\varepsilon_s^\mu = \frac{1}{\sqrt{Q^2}}(q^z,0,0,q^0)$ with $q^\mu = (q^0,0,0,q^z)$ being the virtual photon momentum

$$\begin{aligned}\ell^{\mu\nu}t_{\mu\nu} &= Q^2(t_{11}+t_{22}) + 4\left(\frac{Q^2(1-y)}{y^2} - m_e^2\right)t_{11} \\ &+4\frac{2-y}{y}\ell_x\sqrt{Q^2}\;t_{s1} + Q^2\frac{4(1-y)}{y^2}t_{ss},\end{aligned} \tag{7}$$

where $y \equiv \frac{q^0-q^z}{\ell^0-\ell^z} = \frac{P\cdot q}{P\cdot \ell}$ is identical to the variable defined in (1) in the Lab frame.

In the limit $Q^2 \to 0$ and after azimuthal averaging over φ_4 we recover the unintegrated Weizsäcker-Williams expression

$$\frac{1}{2}\;\frac{\ell^{\mu\nu}t_{\mu\nu}}{Q^4} = \left(\frac{1+(1-y)^2}{yQ^2} - \frac{2y\;m_e^2}{Q^4}\right)\sigma_\perp + \mathcal{O}\left(\left(Q^2\right)^0\right) \tag{8}$$

with $\sigma_\perp = \frac{1}{2y}\,(t_{11}+t_{22})$.

Actually the limit (8) is correct only if $\lim\limits_{Q^2\to 0} t_{ss} = \mathcal{O}(Q^2)$. This is not true if an initial collinearity is present in the partonic tensor (light partons are massless) which leads to the behavior $\lim\limits_{Q^2\to 0} t_{ss} = \mathcal{O}(1)$. This point will be discussed in a forthcoming publication [10].

After these kinematical preliminaries, let us describe the calculation of the HO corrections which uses the phase-space slicing method elaborated in ref. [15]. We outline the strategy only briefly; for more details we refer to [16].

For a generic reaction $1+2 \to 3+4+5$ (fig. 1), at least two particles of the final state, say 3 and 4, have a high $E_\perp$ and are well separated in phase space, while the last one, say 5, can be soft, and/or collinear to any of the four others. Of course on the photon side there is no collinear divergence as long as Q^2 is different from zero. This part of the calculation is related to the virtual photon structure function to be discussed below. In order to extract the other singularities, the phase space is cut into two regions :

(1) Part I where the norm $E_{\perp 5}$ of the transverse momentum of particle 5 is required to be less than some arbitrary value $E_{\perp m}$ taken to be small compared to the other transverse momenta. This cylinder contains the infrared and the initial state collinear singularities. It also contains a small fraction of the final state collinear singularities.

(2) Parts IIa(b) where the transverse momentum vector of particle 5 is required to have a norm larger than $E_{\perp m}$, and to belong to a cone $C_3(C_4)$ about the direction of particle 3(4), defined by $(\eta_5-\eta_i)^2+(\phi_5-\phi_i)^2 \leq R_{th}^2$ $(i=3,4)$, with R_{th} some small arbitrary number. $C_3(C_4)$ contains the final state collinear singularities appearing when 5 is collinear to 3(4).

(3) Part IIc where $E_{\perp 5}$ is required to have a norm larger than $E_{\perp m}$, and to belong to neither of the two cones C_3, C_4. This slice yields no divergence, and can thus be treated directly in 4 dimensions. For this regular part of the calculations we use the cross sections from [17].

The contributions from regions I and IIa, b are calculated analytically in $d = 4-2\varepsilon$ dimensions and then combined with the corresponding virtual corrections (borrowed from DISENT [17]) such that the infrared singularities cancel each other, leaving only the initial (final) state collinear singularities, which are factorized and absorbed into the parton distribution (fragmentation) functions. The $\overline{MS}$ factorization and renormalization schemes are used in this calculation.

After the cancellation, the finite remainders of the soft and collinear contributions

in parts I and IIa, b, c separately depend on large logarithms ln $E_{\perp m}$, $\ln^2 E_{\perp m}$ and ln R_{th}. When combining the different parts, the cancellations of the $E_{\perp m}$ and R_{th} dependent terms occur. Actually, in part I, the finite terms are approximated by collecting all the terms depending logarithmically on $E_{\perp m}$ and neglecting the terms proportional to powers of $E_{\perp m}$. Similarly in parts IIa and IIb we keep only the logarithmic terms ln R_{th}. Therefore the parameter $E_{\perp m}$ must be chosen small enough with respect to $E_{\perp 4}$ so that the neglected terms can be safely dropped. On the other hand, it cannot be chosen too small for then numerical instabilities may occur. Similar remarks are also valid for the R_{th} cut-off.

This approach allows us to build a partonic event generation which is very flexible ; various sorts of observables and experimental cuts being easily handled. More references to this method, which has been used to calculate NLO correction to several photoproduction and hadroproduction reactions can be found in ref. [18].

3 The resolved contribution

As mentioned in the Introduction, the calculation of the HO corrections leads to a contribution proportional to $\log \frac{E_{\perp 4}^2}{Q^2}$ (when $E_{\perp 4}^2 \gg Q^2$), the so-called resolved photon contribution. Indeed, let us consider the contribution associated with Fig. 1b in which we interchange the label 5 and 4. The integration over $E_{\perp 5}$ (the unobserved final quark momentum) produces, among other contributions, a logarithm contribution $\log \frac{E_{\perp 4}^2}{Q^2}$ associated with a configuration in which the final quark is collinear to the virtual photon. More explicitly, we obtain the following expression (for a transversely polarized photon)

$$\begin{aligned} \sigma_\perp &= \frac{\alpha}{2\pi} \int dz \left[z^2 + (1-z)^2\right] \left\{ \int_0^{E_{\perp 4}^2} \frac{dk_\perp^2}{k_\perp^2 - q^2 z(1-z)} \right. \\ &\left. + z(1-z)q^2 \int_0^{E_{\perp 4}^2} \frac{dk_\perp^2}{(k_\perp^2 - q^2 z(1-z))^2} \right\} \widehat{\sigma}(0) dps, \end{aligned} \tag{9}$$

in which we have defined $k = q - p_5$ and $z = \frac{k^{(-)}}{q^{(-)}}$. The cross section of the $2 \to 2$ subprocess is calculated with k on-shell ($k^2 = 0$) and dps is the final partonic phase space of parton 3 and 4. This expression, as well as a similar one for the scalar cross section, will be derived in ref.[10]. A discussion of the second term of (9) (the non-logarithmic piece) is also postponed to this paper. Here we are interested in the term proportional to $\log E_{\perp 4}^2/Q^2$ and in a discussion of the upper limit of the integral in (9).

From (9) we obtain the term

$$\sigma_\perp \simeq \int dz P_{q\gamma}(z) \left\{ \log \ \frac{E_{\perp 4}^2}{Q^2} \right\} \widehat{\sigma}(0) \ dps, \tag{10}$$

(with the definition $P_{q\gamma}(z) = \frac{\alpha}{2\pi}(z^2 + (1-z)^2)$ which defines the quark distribution in the virtual photon

$$q_\gamma(z, E_{\perp 4}, Q^2) = P_{q\gamma}(z) \ \log \ \frac{E_{\perp 4}^2}{Q^2} \ . \tag{11}$$

In expression (11), the quark distribution is calculated with no QCD correction. However when $E_{\perp 4}^2 \gg Q^2$ it becomes important to calculate these corrections and to replace (11) by the LO or NLO expressions of the quark distribution [10, 19, 20, 21].

In this paper we are only interested in the study of the importance of the resolved contribution obtained in the kinematical configuration of the H1 experiment and we content ourselves with the lowest order expression (11). However this expression, obtained in the limit $E_{\perp 4}^2 \gg Q^2$, must be elaborated in order to cover other kinematical configurations as well. When $Q^2 \gtrsim E_{\perp 4}^2$, we cannot neglect the $k_\perp^2$ dependence of $\widehat{\sigma}(k_\perp^2) dps$ which suppresses the logarithmic integration in expression (9). The resolved contribution coming from the collinear configuration can be approximated by the form

$$\sigma_\perp \simeq \int dz \ P_{q\gamma}(z) \log \frac{Q^2 + E_{\perp 4}^2}{Q^2} \ \widehat{\sigma}(0) \ dps, \tag{12}$$

which has the correct limit for $E_{\perp 4}^2 \gg Q^2$ and $E_{\perp 4}^2 \ll Q^2$. In this work we define the resolved contribution by the expression (12), and in Section 4, we shall calculate its numerical importance.

When the lowest order expression (12) is resummed, it must first be removed from the HO corrections. We shall call HO_s the remaining corrections, and we shall say that the subtraction has been performed at the scale $M_\gamma^2 = Q^2 + E_{\perp 4}^2$.

4 Results

In this section we present the results obtained with the NLO code described in sections 2 and 3. We shall compare our predictions with a selected set of H1 data [2] and we shall concentrate on a detailed discussion of the various contributions to the cross section, namely the HO corrections, the virtual photon structure function contribution and the BFKL-like contribution. Here we do not intend to perform a complete phenomenological study of the H1 data [2, 3] that we shall present in a forthcoming publication. We use the MRST99 (higher gluon) [22] distribution functions corresponding to $\Lambda_{\overline{MS}} = 300$ MeV and the KKP fragmentation functions of quarks and gluons in π^0 [23]. The renormalisation and factorization scales are taken equal to $\sqrt{Q^2 + E_{\perp 4}^2}$.

First we study the cross section $d\sigma/dx_{Bj}$ measured by H1 [2] in the range $4.5\ \text{GeV}^2 \leq Q^2 \leq 15\ \text{GeV}^2$ with a lower bound on the transverse energy, in the $\gamma^* - p$ frame, of the forward π^0 given by $E_{\perp 4} > 2.5$ GeV. The HERA proton and electron beams have laboratory energies 820 GeV and 27.5 GeV respectively, and the inelasticity defined in (1) is restricted to the range $.1 < y < .6$. The forward domain in which the meson is observed is given by $5^\circ \leq \theta_\pi^{Lab} \leq 25^\circ$ and $x_\pi = E_\pi^{Lab}/E_{proton}^{Lab} \geq .01$. Then we shall consider other kinematical ranges for Q^2.

The H1 data are compared to our predictions in Fig. 2. The HO contributions from which the resolved contribution has been subtracted (see the discussion in

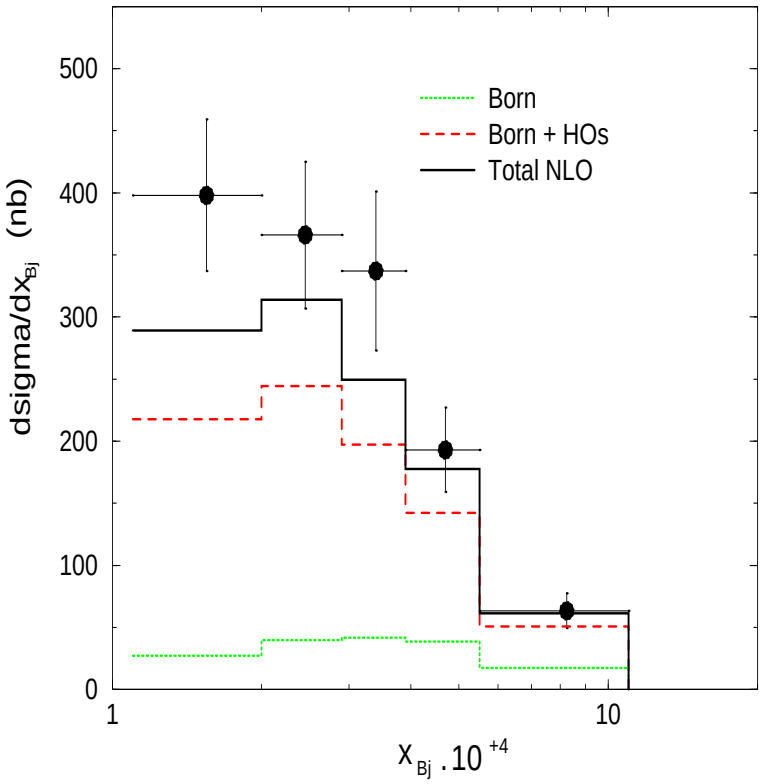

Figure 2: Comparison with H1 data in the range 4.5 GeV$^2 \leq Q^2 \leq$ 15 GeV^2.

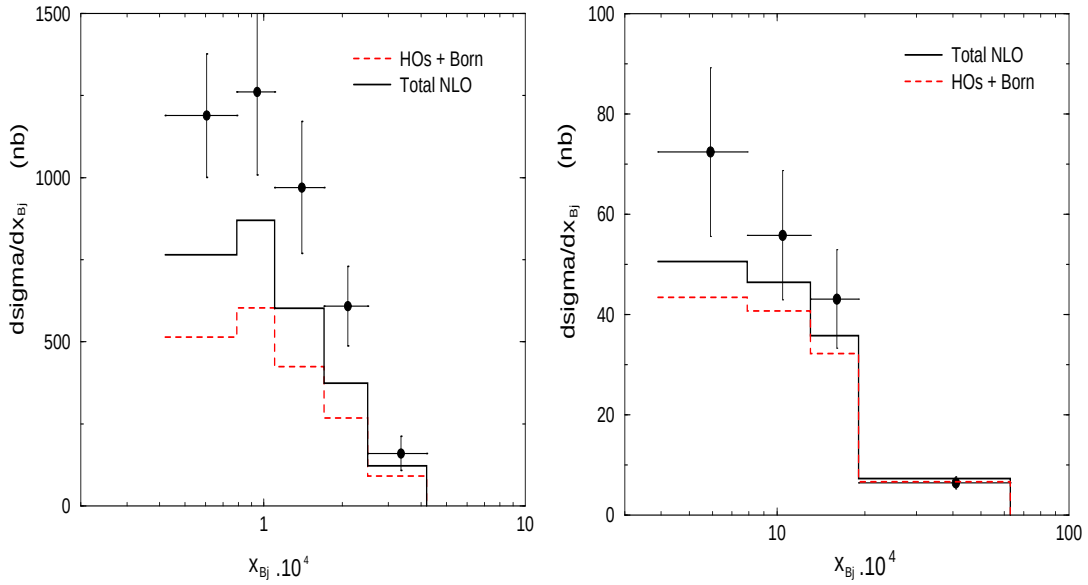

Figure 3: Comparisons with H1 data for two Q^2-ranges : $2 < Q^2 < 4.5$ GeV^2 (left) and $15 < Q^2 < 70$ GeV^2 (right).

section 3) are indicated by HO_s. In Fig. 2 the importance of the HO corrections, especially at small values of x_{Bj} is dramatically visible. As discussed below, it is associated with the opening of new channels.

The resolved component is non-negligible in this range of $E^2_{\perp 4}$ and Q^2. Of course its amplitude depends on the factorization scale, which we discussed in Section 3. We recall that the factorization scale used here is $M^2_\gamma = Q^2 + E^2_{\perp 4}$. It is interesting to look at $< E^2_{\perp 4} >$ and compare it with the value of $< Q^2 >$. According to our calculation $< E^2_{\perp 4} > \simeq 15.3$ GeV^2, which does not depend on the value of x_{Bj}; $< Q^2 > = 6.15$ GeV^2 and 10.36 GeV^2 for the ranges $1.10^{-4} < x_{Bj} < 2.10^{-4}$ and $5.5.10^{-4} < x_{Bj} < 11.0\ 10^{-4}$ respectively. These values lead to a virtual photon structure function proportional to $\log\left(\frac{Q^2+E^2_{\perp 4}}{Q^2}\right) \simeq 1.25$, and 0.91. The dependence of $< Q^2 >$ on x_{Bj} also explains the relative decrease of the resolved component at large x_{Bj}. For two other Q^2 ranges we compare H1 data with theory in Fig. 3. We clearly notice the decrease of the resolved component when Q^2 increases and becomes larger than $E^2_{\perp 4}$.

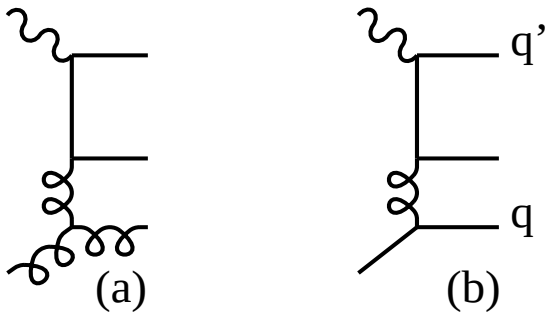

Figure 4: Examples of HO diagrams which contribute to the "BFKL Born" term when the detected hadron is a fragment of the gluon or of the quark q.

Let us end this general discussion of our results by noting that theory underestimates data by a small amount. Nevertheless we must keep in mind that two points are still missing for a more complete comparison. First we have not yet studied the scale dependence of our results which have been obtained for the choice $\mu = M = M_F = M_\gamma = (Q^2 + E_{\perp 4}^2)^{\frac{1}{2}}$, and second, we have not considered HO corrections to the resolved contribution which are known to be large. Indeed we can estimate these corrections by using the Weizsäcker-Williams approximation (8) which is implemented in the photoproduction EPHOX code[18]. From this code we obtain a ratio $HO/Born \simeq 1$ in the kinematical domain corresponding to Fig. 2.

Now we turn to a detailed study of the HO contributions. As expected the two contributions corresponding to the Feynman graphs shown in Fig. 4 are the largest in the forward direction, because of the exchange of a gluon in the t-channel. They also correspond to new subprocesses that are not present at the Born level, as soon as the observed partons are the final gluon or quark q ; therefore they do not possess singular collinear configurations of partons which contribute to the dressing of the distribution and fragmentation functions already present in the Born terms. These graphs, with a trigger on the gluon or quark q, also correspond to the Born terms of the BFKL ladder in which extra gluons are emitted by the t-channel gluon. This is

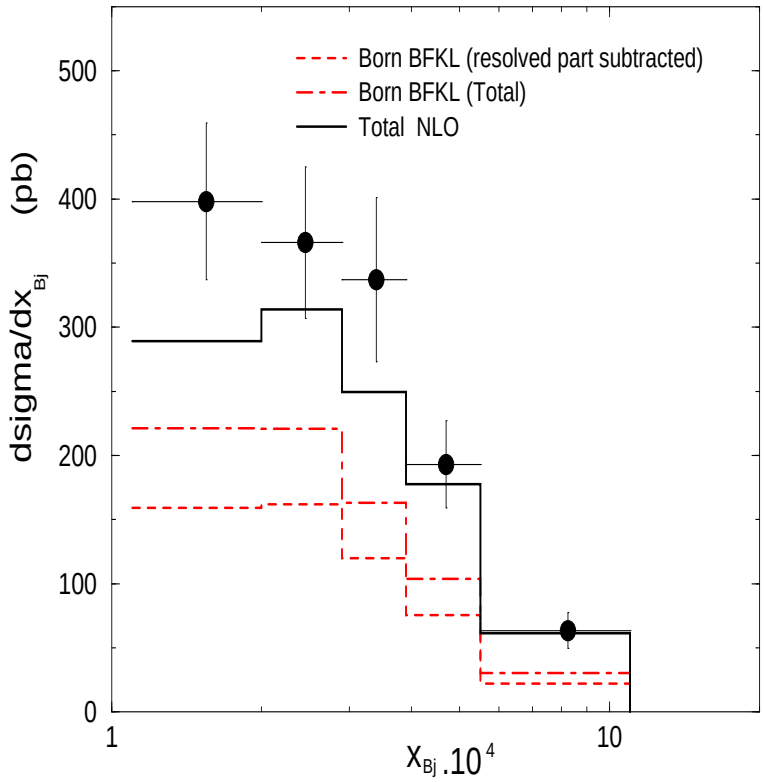

Figure 5: Comparison of BFKL Born contributions with the total NLO cross section and H1 data for 4.5 GeV$^2 \leq Q^2 \leq$ 15.0 GeV^2.

precisely the contribution to the forward cross section [5, 6] that HERA experiments H1 and ZEUS should reveal.

Figure 5 compares our BFKL Born term contributions and the associated resolved contribution with the total NLO cross section $d\sigma/dx_{Bj}$. These contributions represent more than two thirds of the total NLO corrections in the small x_{Bj} region. Actually the BFKL Born result of Fig. 5 also contains contributions of graphs in which, for instance, the outgoing gluon is attached to the quark line. However these contributions are expected to be small as they do not possess the t-singularities (in a physical gauge) associated with the exchange of a gluon. To check this point, we calculated the contributions of the graph shown in Fig. 4b. For a forward trigger on the quark q, we obtain a cross section seven times larger than the one corresponding to a trigger on the quark q' (for $x_{Bj} \sim 2.10^{-4}$). Therefore we estimate that the part

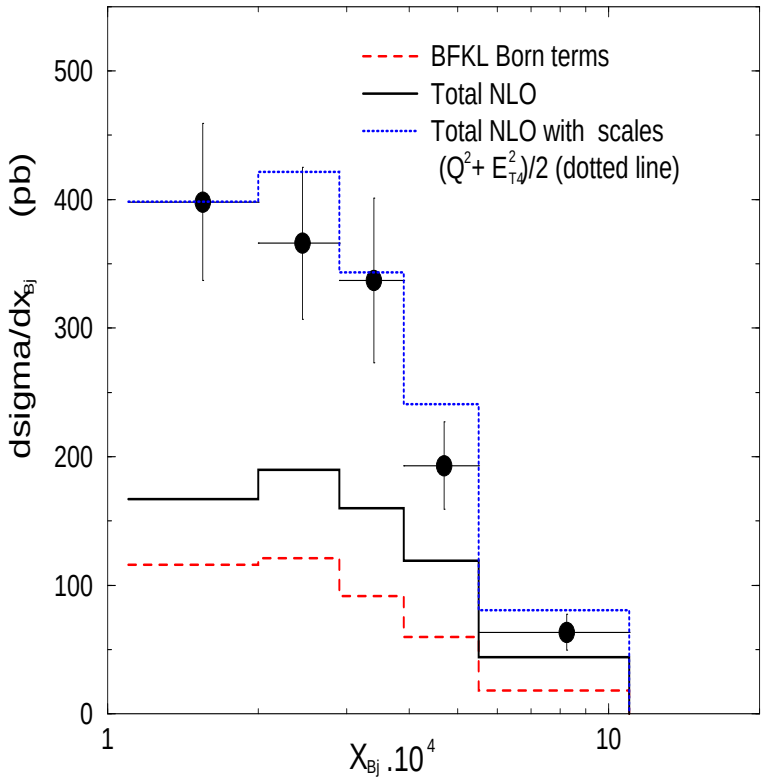

Figure 6: The BFKL Born term contribution and the total NLO cross section with the scales $\mu^2 = M^2 = M_F^2 = p_{\perp 4}^2$. Also shown the total NLO cross section with scales $(Q^2 + E_{\perp 4}^2)/2$ (dotted line) and the H1 data ($4.5 \leq Q^2 \leq 15.0$ GeV^2).

of the curve of Fig. 5 corresponding to the BFKL Born term of Fig. 4 is dominant.

From these results we conclude that the main part of the forward cross section is due to the BFKL Born terms. Although obtained in the course of a NLO calculation, these terms of order $\mathcal{O}(\alpha_s^2)$ represent the Born terms of new channels, namely the $\gamma^* q \to q' \bar{q}' q$ and $\gamma^* g \to q \bar{q} g$ channels. As for any Born terms, we do expect the contributions of those channels to be strongly dependent on the renormalization and factorization scales. Therefore, contrary to our expectations, we are not able to obtain, through our NLO calculations, a total cross section displaying a weak dependence on the renormalization and factorization scales.

Let us be more explicit by studying the effect of the BFKL resummation of the small $\log \frac{1}{x_{Bj}}$ terms which appears when extra gluons are emitted by the t-channel

gluon of Fig. 4 (the BFKL ladder). These contributions have been estimated in ref. [6, 7]; they lead to an enhancement of the BFKL Born cross section by a factor 5 to 10, in obvious contradiction with the data. However the calculations of ref. [6, 7] depend on various cuts and do not include the effect of HO corrections to the leading BFKL results. These corrections are known to be large; this makes the leading results not reliable. A more recent approach [9] includes a part of these HO corrections in its predictions and finds an agreement with H1 data [2]. This last result, obtained with the scales $\mu = M = M_F = p_{\perp 4}$ (p_4 is the momentum of the parton which fragments into the π^0), allows us to make a connection with their approach. Using the same scales we obtain the result of Fig. 6 for the BFKL Born term and for the total cross section. It is obvious that there is room for a BFKL-ladder contribution [9] between the data and the present theoretical prediction.

However the scale $p_{\perp 4}$ is quite large ($< p_{\perp 4} > \simeq 11$ GeV in the H1 kinematics) compared to what is usually used in large-$E_\perp$ reactions. For instance, in the case of π^0 hadroproduction in fixed target experiments, a scale $M \sim E_{\perp 4}/2$ ($< E_{\perp 4} > \simeq 3.6$ GeV in the H1 kinematics) is used in ref. [24] to get an agreement between data and theory. If a similar scale were used here, we would obtain better agreement between data and NLO calculations without any other contributions, as is demonstrated in Fig. 6 for the choice $\mu^2 = M^2 = M_F^2 = \frac{1}{2}(Q^2 + E_{\perp 4}^2)$. It is clear from this discussion that we cannot accurately determine the importance of a BFKL-ladder component in H1 data without calculating NLO correction to the BFKL Born terms considered here or, in other words, without calculating NNLO correction to the electroproduction cross section.

Conclusions similar to the ones of this section have been obtained by Kramer and Pötter in their study of the forward leptoproduction of jets [25].

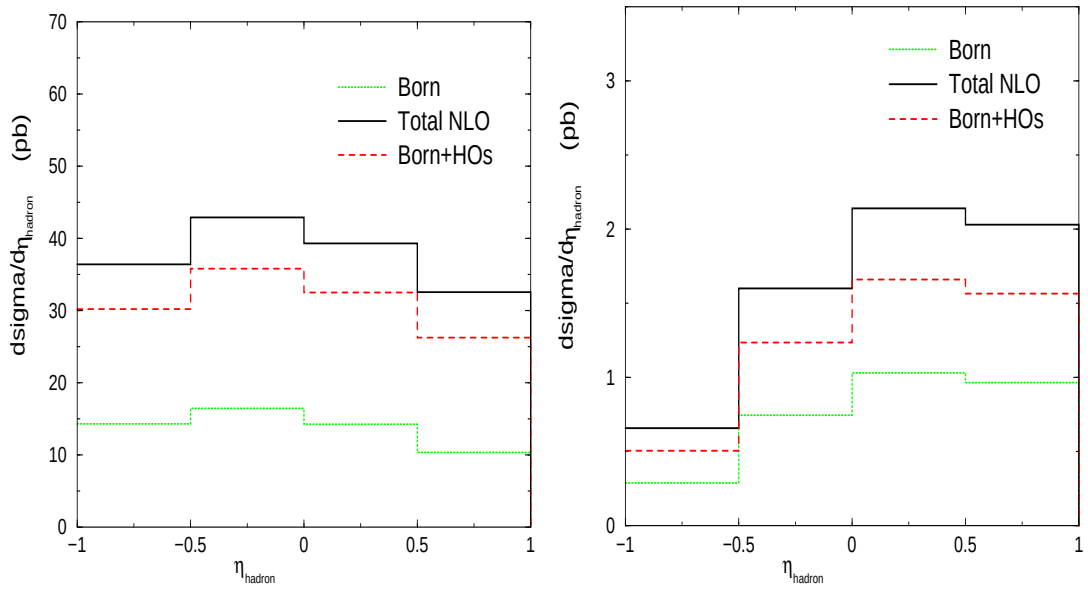

Figure 7: The large-$E_\perp$ π^0 cross section integrated over $E_\perp$ with the cuts $E_\perp >$ 3 GeV/c (left) and $E_\perp > 7$ GeV/c (right).

5 Cross section at central rapidity

In this section we study the leptoproduction of large-$E_\perp$ π^0 in the central region in rapidity (in the laboratory frame) with the aim to reduce the BFKL Born term contributions and, consequently, to have a better control of the HO corrections. Therefore the experimental results obtained in this kinematical domain should provide good tests of QCD and the possibility of measuring the virtual photon structure function.

Let us consider the following kinematical range which has been explored by the H1 collaboration in its measurement of the photoproduction of large-$E_\perp$ hadrons [26], namely $\sqrt{S_{ep}} = 300$ GeV, $.3 \leq y \leq .7$ and $-1 \leq \eta_{hadron} \leq 1$. We study two lower limits for the hadron transverse energy, 3 GeV $\leq E_\perp$ and 7 GeV $\leq E_\perp$, in order, as in ref. [27], to estimate the importance of these cuts on the control of the HO corrections. For Q^2, we choose 5 GeV$^2 \leq Q^2 \leq 10$ GeV^2 which belongs to the range studied by H1 in the measurement of the dijet cross section at low Q^2 [28].

In Fig. 7 we display the cross section $d\sigma/d\eta_{hadron}$ integrated over $E_\perp$ with $E_\perp >$

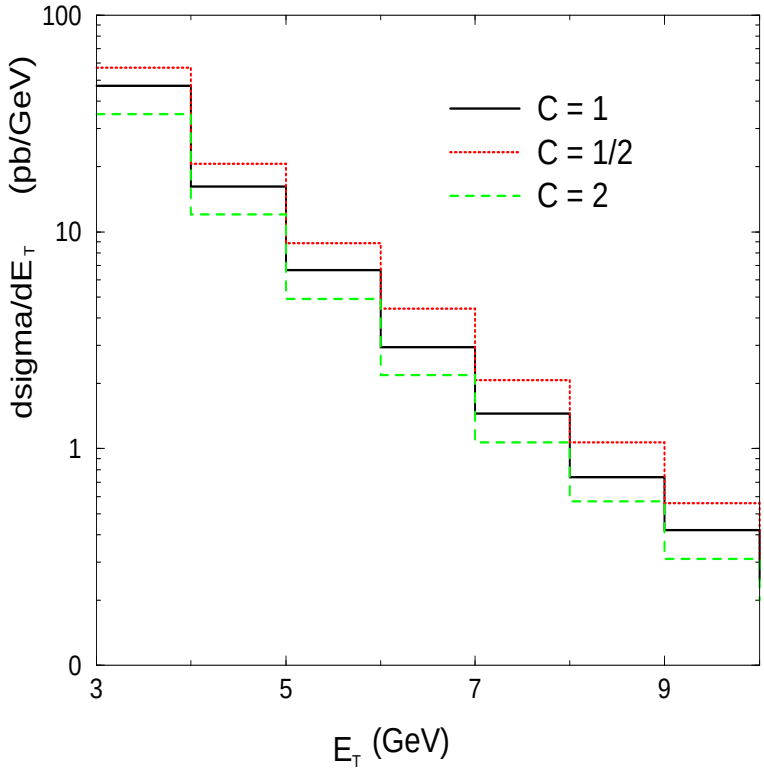

Figure 8: The cross section $d\sigma/dE_\perp$ for three different choices of scales $C\sqrt{Q^2+E_\perp^2}$.

3 GeV (left) and $E_\perp > 7$ GeV (right). All the scales are set equal to $\sqrt{Q^2+E_\perp^2}$. We clearly see the decrease of the ratio $r = \frac{HO_s}{Born}$ when the cut on $E_\perp$ increases, with a value $r \simeq .65$ obtained for $E_\perp > 7$ GeV. On the other hand the ratio of the resolved contribution to the Born contributions increases because of the larger value of $(Q^2+E_\perp^2)/Q^2$ and reaches a value close to 0.5. One must notice that this ratio is much smaller than in photoproduction [27], since the virtuality of the photon suppresses the resolved contribution.

We study the scale variation of the cross-section $d\sigma/dE_\perp$ in Fig. 8. Three predictions, obtained with the scales $\mu = M = M_F = C\sqrt{Q^2+E_\perp^2}$ and $C = \frac{1}{2}, 1, 2$, are displayed. A change of the scales by a factor 4 results in a change of the cross section by a factor 2. Therefore, even at large value of $E_\perp$, the cross section is very sensitive to the scale variation. A similar behavior has been observed in the photoproduction

cross section of large-$E_\perp$ hadrons [27].

6 Conclusion

In this work we have carried out the calculation of HO corrections to the leptoproduction cross section of large-$E_\perp$ hadrons. These corrections are implemented in a parton event-generator offering greater flexibility for the estimation of various observables. Concerning the numerical importance of these corrections, we have focussed on two different kinematical domains, namely the central region in rapidity (in the HERA laboratory frame), and the forward region where we compare our results with H1 data.

In the central region we have found important HO corrections at low $E_\perp$. However these corrections decrease as $E_\perp$ increases with a K-factor (HO/(HO + Born)) of about .5 obtained for $E_\perp > 7$ GeV/c. In the same range the HO corrections contain a non-negligible resolved contribution which should allow experiment to constrain the virtual photon structure function.

In the forward region, we find very large HO corrections due to the opening of new channels related to the BFKL Born terms ; two thirds of the NLO cross section is due to these contributions. These Born terms, and consequently the total NLO cross section, are quite sensitive to scale variations and this forbids any absolute normalization of the cross section. However one must keep in mind that a good agreement between the H1 data and the NLO cross section is obtained with renormalization and factorization scales taken equal to $\sqrt{(Q^2 + E_\perp^2)/2}$.

Because of the scale sensitivity, no firm conclusion can be drawn on the importance of the BFKL resummation in the forward cross section as measured by the H1 collaboration. Clearly such a study requires the calculation of NNLO corrections to the leptoproduction cross section.

Acknowledgements We would like to thank J.-Ph. Guillet for many useful discussions and suggestions. PA and RB would like to thank S. Catani for clarifying many issues regarding the code DISENT in the preliminary stages of this work. RB and RMG would like to thank LAPTH, Annecy and PA and MF would like to thank the Institute of Mathematical Sciences, Chennai and the Indian Institute of Science, Bangalore for their kind hospitality. This work was partially supported by CEFIPRA project 1701-1.

References

[1] H1 Collaboration, S. Aid et al., Nucl. Phys. **B480** (1996) 7.
H1 Collaboration, S. Aid et al., Nucl. Phys. **B485** (1997) 3.
H1 Collaboration, C. Adloff et al., Z. Phys. **C76** (1997) 213. H1 Collaboration, C. Adloff et al., Nucl. Phys. **B538** (1999) 3.

[2] H1 Collaboration, C. Adloff et al., Phys. Lett. **B462** (1999) 440.

[3] H1 Collaboration, paper submitted to EPS 03, Aachen, July 2003.

[4] ZEUS Collaboration, M. Derrick et al., Z. Phys. **C68** (1995) 29.

[5] A. L. Mueller, Nucl. Phys. (Proc. Suppl.) **B18c** (1990) 125.
A. L. Mueller and H. Navelet, Nucl. Phys. **B282** (1987) 727.

[6] J. Bartels, A. de Roeck and M. Loewe, Z. Phys. **C54** (1992) 635.
J. Kwiecinski, A. D. Martin, P. J. Sutton, Phys. Rev. **D46** (1992) 921.
W. K. Tang, Phys. Lett. **B278** (1992) 363.
M. Kuhlen, Phys. Lett. **B382** (1996) 441.
J.Bartels,V.Del Duca,A. De Roeck, D. Graudenz, M. Wüsthoff, Phys. Lett. **B384** (1996) 300.

[7] J. Kwiecinski, S. C. Lang and A. D. Martin, Phys. Rev. **D55** (1997) 1273.

[8] H. Jung, Comp. Phys. Comm. **86** (1995) 147.

[9] J. Kwiecinski, A. D. Martin, J. Outhwaite, Eur. Phys. J **C9** (1999) 611.

[10] M. Fontannaz, in preparation.

[11] L. Trentadue and G. Veneziano, Phys. Lett. **B323** (1993) 201

[12] D. Graudenz, Nucl. Phys. **B432** (1994) 35.

[13] A. Daleo, C. A. Garcia Canal and R. Sassot, Nucl. Phys. **B662** (2003) 334.

[14] A. Daleo and R. Sassot, hep-ph/0309073.

[15] P. Chiappetta, R. Fergani, J. Ph. Guillet, Z. Phys. **C69** (1996) 443.

[16] T. Binoth, J. Ph. Guillet, E. Pilon, M. Werlen, Eur. Phys. J **C16** (2000) 311.

[17] E.B.Zijlstra and W.L. van Neerven, Nucl. Phys. B383(1992)525. We use the matrix elements contained in the DISENT code of S. Catani and M. H. Seymour, Nucl. Phys. **B485** (1997) 291. E : **B510** (1997) 503. S.Catani and M.H.Seymour, Workshop on Future Physics at HERA, DESY(1996), hep-ph/9609521.

[18] "The PHOX Family", a base of NLO FORTRAN codes, available from http://www.lapp.in2p3.fr/lapth/PHOX_FAMILY/main.html.

[19] M. Klasen, G. Kramer and B. Pötter, Eur. Phys. J **C1** (1998) 261.

[20] G. Kramer and B. Pötter, Eur. Phys. J **C5** (1998) 665.
B. Pötter, Comput. Phys. Commun. **119** (1999) 45.

[21] J. Chýla and M. Taševský, Eur. Phys. J **C18** (2001) 723.

[22] A. D. Martin, R. G. Roberts, W. J. Stirling and R.S. Thorne, Eur. Phys. J **C23** (2002) 73.

[23] B. A. Kniehl, G. Kramer, B. Pötter, Nucl. Phys. **B582** (2000) 514.

[24] P. Aurenche, M. Fontannnaz, J. Ph. Guillet, B.A. Kniehl, M. Werlen, Eur. Phys. J **C13** (2000) 347.

[25] G. Kramer and B. Pötter, Phys. Lett. **B453** (1999) 295.

[26] H1 Collaboration, C. Adloff et al., Eur. Phys. J **C10** (1999) 363.

[27] M. Fontannaz, J. Ph. Guillet, G. Heinrich, Eur. Phys. J **C26** (2002) 209.

[28] H1 Collaboration, Measurement of dijet cross section at low Q^2 at HERA, submitted to the International Europhysics Conference on High Energy Physics, EPS03, July 2003, Aachen.